(Preprint) AAS 26-932

APPLICATIONS OF THE WEIGHTED BIRKHOFF AVERAGE IN ASTRODYNAMICS

Addisyn Randolph[*], J. D. Mireles James[*], Luke Peterson [†]

Quasi-periodic orbits display predictable motion which can be exploited in a wide range of applications in spacecraft mission design. The parameterization method is a state-of-the-art strategy for computing invariant tori and their manifolds in dynamical systems by solving an invariance equation via a Newton-like scheme; however, this is a numerically sensitive procedure requiring the rotation number and a good initial approximation of the torus. Weighted Birkhoff averages (WBA) resolve this problem; hence, the goal of this paper is to compute high-order Fourier expansions of quasi-periodic orbits in the Circular Restricted 3-Body Problem (CR3BP) by combining the method of weighted Birkhoff averages with the parameterization method. The parameterization method describes the invariant torus as the solution of a certain nonlinear functional equation, which we solve using an iterative scheme. Two critical steps then are (1) accurately computing the rotation vector and (2) finding a good initial approximation of the torus so that the iterative method converges. Both tasks are performed efficiently using the WBA. When the torus is unstable, we also compute parameterizations of the local stable/unstable invariant manifolds.

INTRODUCTION

The goal of this paper is to describe a method for computing quasi-periodic orbits (QPO) of the planar Circular Restricted 3-Body Problem CR3BP using the parameterization method via weighted Birkhoff averaging. We also compute QPOs in the spatial problem with their attached stable and unstable manifolds.

As the number of multi-body missions increases, so does the need for robust computational strategies to generate baseline trajectories around Lagrange points and primary-centered orbits. For example, the 1978 ISEE-3/ICE mission was the first near libration point satellite to utilize the Sun-Earth L_1 halo orbit.[1] Recently, in 2022, the CAPSTONE mission successfully demonstrated the use of a Near Rectilinear Halo Orbit (NRHO) intended for NASA's Lunar Gateway mission[2] and the Artemis 1 mission put the Orion vehicle into a lunar Distant Retrograde Orbit (DRO).[3] Missions still being planned include the Comet Interceptor (Comet-I) mission which plans to launch in 2029 and idle in a Sun-Earth L_2 quasi-halo orbit[4] and the Gateway program which planned to utilize a lunar NRHO.[5]

Quasi-periodic orbits display predictable bounded motions across these multi-body systems and, because of this, they are often used for applications in mission design. The ISEE-3/ICE, CAPSTONE, and Artemis 1 illustrate the utility of periodic solutions in mission design; however, periodic motions form only a small subset of the regular motions. Invariant tori, while more difficult

[*]Department of Mathematics and Statistics, Florida Atlantic University. Partially supported by NSF DMS – 2307987
[†]Department of Aerospace Engineering and Engineering Mechanics, University of Texas at Austin.

to compute, are infinitely more abundant than periodic orbits, offering mission designers more options and more realistic design strategies. For example, the Solar Heliospheric Observatory (SOHO) has been orbiting the Sun-Earth libration point L_1 on a quasi-periodic halo orbit[6] since 1996. In 2015, the Deep Space Climate Observatory (DSCOVR) was put in a Sun-Earth L_1 quasi-periodic Lissajous orbit.[7] Restrepo, Russell, and Lo investigated using Lissajous orbits and their manifolds to generate landing trajectories on the surface of Europa.[8] The bounded motion of a quasi-periodic orbit makes it a possibility for spacecraft formation flying as explored by Barden and Howell,[9] and Baresi.[10] The references just listed discuss many additional examples, and a much more complete discussion of the pre-Twenty-First Century literature is found elsewhere.[11–14]

One method for computing quasi-periodic orbits is the parameterization method which is a state-of-the-art strategy for computing invariant tori and their manifolds in dynamical systems. The idea behind the method is to find a (truncated) Fourier expansion which approximately solves a certain dynamical conjugacy equation (Eq. (2) and Eq. (3)). Other methods for computing QPOs include the work done by Jorba and Olmedo[15] where they compute Fourier series describing the invariant curve in a Poincaré section of the torus. Gómez and Mondelo[16] and Kumar et al.[17] also compute the Fourier expansion of a curve on a surface of section of the torus using a multiple shooting method. In this work we use the parameterization method to compute the full torus and its manifolds instead of restricting to a section. Schilder et al.[18,19] computed invariant tori of flows by solving an invariance equation over a grid of points in phase space rather than Fourier space.

The invariance equation is solved iteratively using a harmonic balance/Newton scheme. The functional equation conjugates the dynamics on the torus to constant rotations,[20] and two essential steps for implementing this method are (1) accurately computing the rotation vector of the torus and (2) finding a good initial approximation of the torus so Newton converges. In the remainder of the present work, we consider two different strategies for this:

- (A) **Data-driven approach:** near a stable torus, we perform a long simulation of a quasi-periodic orbit. From its numerically computed time series we extract ergodic observables like the components of the rotation vector and the approximate Fourier coefficients by averaging. This is discussed in some detail in Section *Weighted Birkhoff Averaging*.
- (B) **Local analysis:** for an unstable torus near a saddle $\times$ center $\times$ center equilibrium solution, we obtain the rotation vector as well as approximate Fourier coefficients for a two-dimensional torus from a normal form analysis.

The Weighted Birkhoff average (WBA) is an averaging method characterized by its rapid convergence and is used to distinguish between chaos and quasi-periodic motion and to compute observables like rotation numbers and Fourier series coefficients.[21,22] Authors such as Blessing and Mireles-James[23] and Boodram et al.[24] applied WBA to compute rotation numbers for invariant circles of the standard map and Keplerian map respectively. Ruth et. al applied WBA to classify trajectories as integrable or chaotic and computed Fourier series with a WBA and least squares approach in the CR3BP.[25] The advantage of WBA is that it uses only a single long time series, usually an orbit on the invariant torus or circle, to compute the rotation number and approximate the Fourier coefficients. The approximate Fourier coefficients are then refined using a Newton scheme based on the parameterization method. Blessing and Mireles-James used WBA and the parameterization method to compute invariant circles for maps.[23] The approach presented here extends their work to 2-dimensional tori for Hamiltonian differential equations in particular, the CR3BP. We compute one rotation number using the WBA method in a Poincaré section and the second rotation number is obtained by averaging return times to the section.

Since the planar CR3BP is a 2-DOF system, invariant tori are maximally dimensional–in this sense, they are called Lagrangian tori and are "sticky," so that points near a torus stay near the torus for a long time.[26] This results in reliable averages for the WBA method. The spatial problem, on the other hand, admits unstable (hyperbolic) invariant tori. For such a torus, nearby points diverge exponentially fast in forward and backward time and a long time series near the torus, needed for WBA, is difficult to obtain via direct simulation. An alternative is to use a normal form to find tori near a base invariant object like an equilibrium or periodic orbit. See for example, the many works of Jorba,[27–29] as well as recent work by Peterson.[30,31] The limitation of normal forms is that they are intrinsically local; the Taylor remainder is small only in a small neighborhood of the base invariant object, but we only need an approximation for Newton to correct it.

Once we have computed a single torus using either method (A) or (B) described above, we can compute a nearby Torus by making a small change to either the energy, one of the rotation numbers, or a parameter of the system (the mass ratio in the case of the CR3BP). Using the "old" torus as an initial guess at the new parameters, we run Newton again. Should the computation converge, we can of course repeat the procedure. This strategy can be combined with various predictor corrector schemes to improve continuation step size.

The paper is outlined as follows. First, we establish some preliminaries, reviewing the dynamical model used, various parameterization methods for computing quasi-periodic orbits and their stable/unstable manifolds, as well as weighted Birkhoff averages. Combining these techniques, we derive an algorithm to compute 2-dimensional quasi-periodic invariant tori using WBAs or taking a semi-analytical solution via normal form as the initial guess for the derived Newton method. Moreover, we similarly construct a routine to compute the stable and unstable manifolds for the QPO via Newton method. Then, we illustrate the performance of these algorithms through two main test cases: a planar Moon-centered orbit, and L_2 Lissajous orbits. We present error analysis alongside the results and discuss future directions for the present work.

PRELIMINARIES

In this section we provide the necessary background the remainder of this work. We begin with presenting the dynamical model of the CR3BP and then explain the parameterization method for invariant tori and their manifolds. In the last part, we explain the method of weighted Birkhoff averaging as used here.

Dynamical Model

The CR3BP describes the motion of a massless particle under the attraction of two larger masses m_1, m_2, which are called the primaries. The gravitational attraction of the particle on the primaries is neglected since its mass is taken to be infinitesimal. In astrodynamics, this model is often used to study the motion of a satellite in the Earth-Moon system.[32] We take μ and $1-\mu$ to be the normalized masses of the smaller and larger primary, respectively. We also take the usual reference frame: the origin is the mutual barycenter of the primaries and the primaries are located at $(1-\mu, 0, 0)$ and $(-\mu, 0, 0)$ respectively.[32] The equations of motion of the massless particle are

$$\ddot{x} - 2\dot{y} = \Omega_x, \qquad \ddot{y} + 2\dot{x} = \Omega_y, \qquad \ddot{z} = \Omega_z, \tag{1}$$

where

$$\Omega = \frac{1}{2}(x^2 + y^2) + \frac{1-\mu}{r_1} + \frac{\mu}{r_2} + \frac{1}{2}\mu(1-\mu),$$

and r_1, r_2 are the distances from each primary, defined by

$$r_1 = \sqrt{(x+\mu)^2 + y^2 + z^2} \qquad r_2 = \sqrt{(x+\mu-1)^2 + y^2 + z^2}.$$

This system has one integral of motion called the Jacobi constant, C. By defining the momenta as $\rho_x = \dot{x} - y$, $\rho_y = \dot{y} + x$, and $\rho_z = \dot{z}$, the Hamiltonian governing the motion of the particle is

$$H = \frac{1}{2}(\rho_x^2 + \rho_y^2 + \rho_z^2) + y\rho_x - x\rho_y - \frac{1-\mu}{r_1} - \frac{\mu}{r_2}$$

The Jacobi constant is related to the Hamiltonian by $C = -2H$.

For ease of notation, we let $U = \frac{1-\mu}{r_1} + \frac{\mu}{r_2}$, and then we can write the vector field $F : \mathbb{R}^6 \to \mathbb{R}^6$ version of (1) as

$$F(x, y, z, \rho_x, \rho_y, \rho_z) = \begin{pmatrix} \rho_x + y \\ \rho_y - x \\ \rho_z \\ \rho_y + U_x \\ -\rho_x + U_y \\ U_z \end{pmatrix},$$

where U_x, U_y, U_z are the partials of U with respect to x, y, and z, respectively. Then the differential equation deifning the spatial CR3BP is given by

$$\dot{X} = F(X)$$

with F as above. It is sometimes beneficial to look instead at the planar case where the motion of the particle is restricted to the x-y plane so $z = \dot{z} = 0$. The phase space then lies on $\mathbb{R}^4$ instead of $\mathbb{R}^6$. In this work, we begin with the planar case and then move to the spatial case.

Parameterization Method for Invariant Tori

The parameterization method is a strategy for computing invariant tori and invariant manifolds introduced by Cabré et al.[33–35] The idea is to study an invariance equation describing the invariant torus which is parameterized as an unknown formal series. One then solves for the torus via a Newton-like scheme. In this section and the next, we discuss in more detail how we use this method. Let $F\colon \mathbb{R}^6 \to \mathbb{R}^6$ be the vector field describing the dynamics of the CR3BP and suppose that $\gamma\colon \mathbb{R} \to \mathbb{R}^6$ is a solution of the differential equation

$$\gamma'(t) = F(\gamma(t)), \qquad t \in \mathbb{R}.$$

We say that γ is a quasi-periodic orbit if the image of γ is dense in a torus. Quasi-periodic orbits necessarily involve infinite forward and backward in time asymptotics, and it is in fact easier to shift focus and study the resulting invariant torus directly. The idea of the parameterization method[36] is that this can be done by looking for a mapping $K\colon \mathbb{T}^2 \to \mathbb{R}^6$ conjugating the flow generated by F to the flow on $\mathbb{T}^2$ generated by an irrational 2-dimensional (constant) rotation vector field

$\hat{\omega} = (\omega_1, \omega_2)^T$. We refer to the components of $\hat{\omega}$ as the *rotation numbers*. Note that if $\theta = (\theta_1, \theta_2)$ is an initial condition in $\mathbb{T}^2$ then the orbit of θ generated by $\hat{\omega}$ is

$$\theta(t) = \begin{pmatrix} \theta_1 + t\omega_1 \\ \theta_2 + t\omega_2 \end{pmatrix}.$$

The system of (partial differential) equations enforcing the dynamical conjugacy (on the level of vector fields) is given by

$$\omega_1 \frac{\partial}{\partial \theta_1} K(\theta_1, \theta_2) + \omega_2 \frac{\partial}{\partial \theta_2} K(\theta_1, \theta_2) = F(K(\theta_1, \theta_2)) \tag{2}$$

Geometrically, this equation says that the push forward of the model vector field $\hat{\omega}$ by DK is equal to the restriction of the given vector field F on the image of K. The dynamical significance is that when K satisfies the conjugacy of Equation (2), then it must also satisfy the flow conjugacy

$$\Phi_t(K(\theta)) = K(\theta + t\hat{\omega}), \tag{3}$$

where Φ_t denotes the flow generated by F and $\theta = (\theta_1, \theta_2)^T$. If K is periodic in each variable and ω_1, ω_2 are mutually irrational modulo 2π, then the image of the orbit $\theta(t)$ is dense in the 2-torus covered by the image of K. We note that in the planar CR3BP all tori are either periodic orbits or 2-tori, and that an invariant 2-torus cannot be unstable, as it has maximal dimension (e.g., a 2D torus comes in a 2-parameter family, and the phase space in the planar CR3BP is 4-dimensional). Similarly, in the spatial problem, 3-tori cannot be unstable, and it is only 2-tori that can have stable/unstable manifolds, enabling low-energy transport.

Parameterization Method for Stable/Unstable Manifolds

Suppose we have computed an invariant torus parameterized by $K : \mathbb{T}^2 \to \mathbb{R}^6$ and satisfying Eq (2). If K has a stable (unstable) Floquet multiplier λ, then we want to compute the attached stable (unstable) manifold. Following Haro,[36] we have that a parameterization of a local stable (unstable) manifold solves the invariance equation

$$F(Q(\theta, \sigma)) = D_\sigma Q(\theta, \sigma)\lambda\sigma + D_\theta Q(\theta, \sigma)\hat{\omega} \tag{4}$$

where F is the CR3BP vector field and $\hat{\omega}$ is the rotation vector. We make a Fourier-Taylor ansatz

$$Q(\theta, \sigma) = \sum_{k=0}^{\infty} a_k(\theta)\sigma^k, \tag{5}$$

where for each $k = 1, 2, ...,$ $a_k : \mathbb{T}^2 \to \mathbb{R}^6$ is an unknown Fourier series. Substituting Eq (5) into Eq (4), notice that $Q(\theta, 0) = a_0(\theta) = K(\theta)$. The stability of the torus, governed by λ, is found by looking at the first-order equation

$$-D_\theta a_1(\theta)\hat{\omega} + DF(K(\theta))a_1(\theta) = \lambda a_1(\theta) \tag{6}$$

We can solve for λ, the Floquet multiplier, and $a_1(\theta)$, the invariant vector bundle, as an eigenvalue eigenfunction pair of the linear operator L, defined by it's action

$$L[W(\theta)] := -D_\theta W(\theta)\hat{\omega} + DF(K(\theta))W(\theta) \tag{7}$$

If Q satisfies Eq (4) the first order constraints: $a_0(\theta) = K(\theta)$ and Eq (6), then for all $\theta_1, \theta_2 \in \mathbb{T}^2$ and $\sigma \in [-1, 1]$

$$Q(\theta_1 + t\omega_1, \theta_2 + t\omega_2, e^{\lambda t}\sigma) = \Phi(Q(\theta_1, \theta_2, \sigma), t)$$

where Φ is the flow generated by F. Then, if $\lambda < 0$, $image(Q)$ is a subset of the local stable manifold of K. Similarly, if $\lambda > 0$ and $image(Q)$ is a subset of the local unstable manifold of K.

Weighted Birkhoff Averaging

Since we will consider 2D tori in the present work, we normalize the rotation vector as $\hat{\omega} = \frac{1}{T}(\omega, 1)$ where T is the average flying time of the torus, and ω is the rotation number from the discrete time Poincaré map.[20] Defining it in this way allows us to reduce the dimension of the problem and look for invariant circles before computing the torus. See for example Figure 1. In these figures, coherent rings indicate invariant circles of the Poincaré section, and "TV static" indicates chaotic/mixing dynamics. Such rings appear when the surface of section cuts an invariant torus transversely of the full system, so that we can read the initial conditions of a quasi-periodic solution directly off of the picture. The rotation number of the invariant circle is found by applying the Birkhoff Ergodic Theorem and weighted Birkhoff averages.[21,23]

The general idea behind this averaging scheme is as follows. Let F be the vector field for the CR3BP and $\mathcal{T}$ the rotation map on the circle defined by

$$\mathcal{T}(\theta) = \theta + \hat{\omega} \mod 2\pi$$

the Birkhoff average is defined as

$$B_N(f)(\theta) = \frac{1}{N} \sum_{n=0}^{N-1} F(\mathcal{T}^n(\theta)).$$

The Birkhoff Ergodic Theorem[21] states that

$$\lim_{N \to \infty} \frac{1}{N} \sum_{k=0}^{N-1} F(\mathcal{T}^k(x)) = \int_{T^2} f d\mu. \tag{8}$$

In other words, the time average of F along the $\mathcal{T}$-orbit of almost every x is equivalent to the spatial average of F over $\mathbb{T}^2$. Thus, the Birkhoff Average can be considered as an approximation of the integral. This average has very slow convergence and is not suitable for numerical computations.[21] Instead, the weighted average defined as

$$WB_N(\mathcal{T}, f)(\theta) = \sum_{n=0}^{N-1} \hat{w}_{n,N} f(\mathcal{T}^n(\theta)) \tag{9}$$

$$\hat{w}_{n,N} = \frac{w\left(\frac{n}{N}\right)}{\sum_{j=0}^{N} w\left(\frac{j}{N}\right)}$$

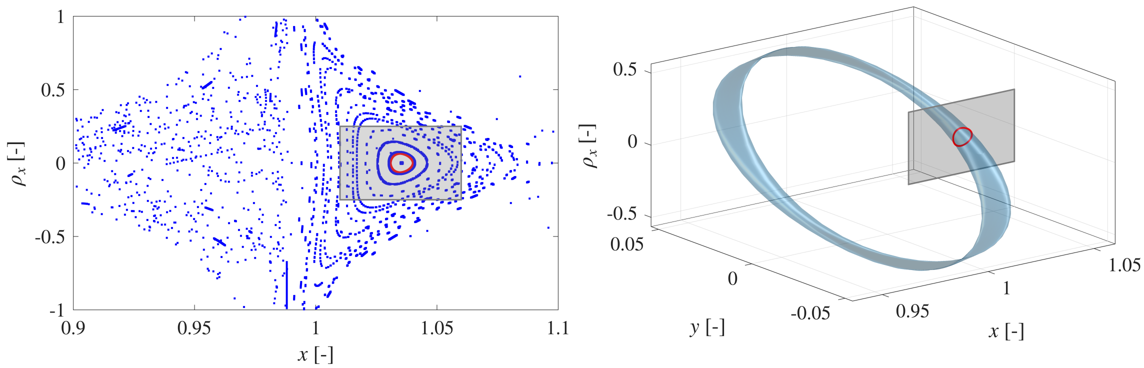

Figure 1: Poincaré map for the planar CR3BP with Earth/Moon mass ratio $\mu = 0.01215$ and $H = -1.58$. The red line represents the orbit starting at $p_0 = (1.04, 0)$ which is realized as the red invariant circle on the 2D torus on the right.

where $w(t)$ is the C^∞ bump function defined by

$$w(t) = \begin{cases} \exp\left(\frac{1}{t(t-1)}\right), & \text{for } t \in (0,1) \\ 0, & \text{for } t \notin (0,1) \end{cases} \tag{10}$$

has super convergence to the spatial average (exponential versus linear).

The weighted Birkhoff average is be used to compute the rotation number, ω, of the Poincaré map. The Poincaré map is constructed by fixing the Hamiltonian, H, and choosing a Poincaré section, typically the positive x-axis. An initial point p_0 in the section is flowed for time $\tau(p_0)$ which is the time it takes for p_0 to return to the section. We can define the map implicitly by

$$P(p_0) = \Phi_{\tau(p_0)}(p_0)$$

The rotation number for the invariant circle is the average rotation between any two iterations of the map. Given a finite orbit from the Poincaré map, $\text{orbit}_{M,F}(p_0) = \{p_j\}_{j=0}^M \subset \mathbb{R}^2$, we compute the associated angle data $\{\theta_j\}_{j=0}^M$ where θ_j is the angle between p_j and the center of the invariant circle. The truncated sum

$$\omega_M = \sum_{m=0}^{M-1} \hat{w}_{m,M}(\theta_{m+1} - \theta_m) \mod 1 \tag{11}$$

converges rapidly to ω, the rotation number of the circle.[21] The idea is that since the rotation number is a topological invariant, we detect it by observing the dynamics on the embedding of the circle in phase space. Blessing and Mireles-James use this to compute the rotation number of an invariant circle but also go further and compute the parameterization of the invariant circle for various explicit examples.[23]

Another application of the weighted Birkhoff average is to compute an approximation of the Fourier coefficients of K.[23] The Fourier expansion of $K : \mathbb{T}^2 \to \mathbb{R}^6$ is

$$K(\theta) = \sum_{n \in \mathbb{Z}^2} k_n e^{2\pi i n \cdot \theta}$$

where for every $n \in \mathbb{Z}^2$ the n-th Fourier coefficient is

$$k_n := \int_{T^2} K(\theta) e^{-2\pi i n \cdot \theta} d\theta$$

If $\{p_j\}_{j \geq 0}$ is a set of points on the quasi-periodic orbit such that $p_{j+1} = \Phi_1(p_j)$ where Φ_1 is the time-1 flow map, then the quantity

$$WB_M[K(\theta)e^{-2\pi i n \cdot \theta}] = \sum_{j=0}^{M-1} \hat{w}_{j,M} p_j e^{-2\pi i j (n \cdot \hat{\omega})} \tag{12}$$

converges rapidly to the $n \in \mathbb{Z}^2$ Fourier coefficient of the parameterization of the torus.[21]

COMPUTATION OF 2D TORI VIA NORMAL FORM AND BIRKHOFF AVERAGES

In the following, we detail the harmonic balance equation in the CR3BP and how to compute the rotation vector. Then we present algorithms for computing a QPO in both the planar and spatial case of the CR3BP.

Harmonic Balance

Let us first consider the planar case of the CR3BP where $z = \dot{z} = 0$. We wish to find a parameterization $K : \mathbb{T}^2 \to \mathscr{T} \subset \mathbb{R}^4$ that satisfies the invariance equation, Eq (2). Using the parameterization method, we treat K as an unknown to the equation and solve a Newton like scheme. Since K is doubly periodic, we can write it as a Fourier expansion

$$K(\theta_1, \theta_2) = \sum_{m \in \mathbb{Z}} \sum_{n \in \mathbb{Z}} k_{m,n} e^{2\pi i (m\theta_1 + n\theta_2)}$$

where $k_{m,n} \in \mathbb{R}^4$ are the Fourier coefficients. Then, the coefficients are defined as

$$k_{m,n} = \int_0^1 \int_0^1 K(\theta_1, \theta_2) e^{-2\pi i (m\theta_1 + n\theta_2)} d\theta_1 d\theta_2$$

To compute an approximation of the Fourier coefficients, we compute M many points on the quasi-periodic orbit $\{p_k\}_{k=0}^M = \{\Phi_1^k(p_0)\}_{k=0}^M$ with Φ_1 as the time-1 flow map and $\Phi_n \equiv \Phi_1^n$. Note that

$$\begin{aligned}
p_0 &= K(\theta_0) \\
p_1 &= \Phi_1(p_0) = \Phi_1(K(\theta_0)) = K(\theta_0 + t\hat{\omega}) = K(\theta_1) \\
&\vdots \\
p_n &= \Phi_1(p_{n-1}) = \Phi_1(K(\theta_{n-1})) = K(\theta_{n-1} + t\hat{\omega}) = K(\theta_n)
\end{aligned}$$

since K satisfies Eq (3). Then we compute the approximation using Eq (12).

In the spatial CR3BP, the parameterization of an invariant 2D torus is $K : \mathbb{T}^2 \to \mathbb{R}^6$. Now, the tori are hyperbolic, making it very difficult (maybe impossible) to compute a long enough orbit needed for the Birkhoff averaging. Using numerical integration, the orbit would eventually fly away from the torus. Here we employ the normal form method as described by Peterson and Scheeres[30] based on the computational method of Jorba[28] to seed the Newton scheme. The normal form Hamiltonian is made by putting the Hamiltonian in a nice form which gives us action-angle variables, I_1, I_2, I_3, to parameterize a semi-analytic solution. Since the normal form is an approximation to the real system, the torus generated by these variables is also an approximate torus of the CR3BP Hamiltonian. Thus, it serves as a suitable initial guess.

Since the collinear Lagrange points have stability type saddle $\times$ center $\times$ center, I_1 corresponds to the saddle integral and I_2, I_3 to the center integrals. Quasi-periodic motion occurs when $I_1 = 0$ and $I_2, I_3 > 0$. We choose appropriate values for I_2, I_3 and generate the torus for values of $\theta_2, \theta_3 \in [0, 2\pi]$. This generates points on the torus to which we apply DFT. This gives us an approximation of the Fourier coefficients.

Computing the Rotation Vector

We must also find the rotation vector, $\hat{\omega} = 1/T(\omega, 1)$ of the torus where ω is the rotation number of the Poincaré map and T is the average flying time of the torus. The average flying time, T, of the torus is computed using Birkhoff Averaging. Let $\tau(x_j)$ be the time it takes for a trajectory starting at $x_j \in \mathbb{R}^4$ in the Poincaré section to return to the section. If $\{\tau(x_j)\}_{j\geq 0} = \{T_j\}_{j\geq 0}$ then

$$T_M = \sum_{j=0}^{M-1} \hat{w}_{m,M} T_j \tag{13}$$

is an approximation of the average flying time truncated at some large M.

The rotation number of the Poincaré map is computed from the orbit data, $\text{orbit}_{M,F}(p_0) = \{p_j\}_{j=0}^{M}$ using Eq (11). To obtain angle data, we choose some point q_0 inside the invariant circle and compute the following

$$\begin{pmatrix} x_j \\ y_j \end{pmatrix} = \xi_j = p_j - q_0 \tag{14}$$

$$\theta_j = \frac{\text{atan4}(y_j, x_j)}{2\pi} \tag{15}$$

Where atan4 is a function defined in MATLAB to be a four quadrant arctangent function. It returns an angle between ξ_j and the x-axis between 0 and 2π. Here, the difference in angles is the *oriented difference*

$$\theta - \sigma = (\theta - \sigma) - \lfloor \theta - \sigma + 1/2 \rfloor$$

which gives the smallest angle needed to be added to θ to get to σ and can be either positive or negative.[23]

Choosing the initial point, p_0, on the invariant circle is a much studied problem, as noted by Blessing and Mireles-James. One way is to examine plotted orbit segments for different values of M and visually observe if the orbit densely fills the circle. Another method is to check the convergence of the rotation number.[37] We increase M and note how quickly the rotation number converges. See Table 1. Rotation numbers with faster convergence are more likely to have been sampled from an invariant circle. In this work, we choose p_0 by observing the plot of the Poincaré map and picking a point that lies on or close to what appears to be a circle on the plot. See Figure 1. Then, using the previously mentioned methods, we check if it indeed lies on an invariant circle.

In the spatial case, because the tori are hyperbolic, we cannot easily compute a long orbit to compute the rotation number, ω. The initial data for the spatial case comes from performing a normal form transformation of the CR3BP. After the action-angle coordinate transformations, the rotation numbers are found as

$$\omega_j = \dot{\theta}_j = \frac{\partial H}{\partial I_j} \quad \text{for } j = 2, 3$$

The rotations from the normal form have periods of 2π, so we normalize it to $\hat{\omega} = 1/2\pi(\omega_2, \omega_3)^T$.

Newton Method Set-up for QPO

The parameterization treats the torus K as an unknown to Eq (2) and solves it via a Newton iteration scheme. The initial guess for the Newton scheme can be computed using methods mentioned in the previous sections. In order for Newton to converge, it must be applied to a system that has an isolated solution.

The parameterization, K, is only unique up to a phase. That is, if K satisfies Eq (2), then for any fixed ϵ, $K_\epsilon(\theta) = K(\theta + \epsilon)$ is also a parameterization. The frequency vector, $\hat{\omega}$, is also only defined up to a unimodular matrix $A \in Z^{2\times 2}$. The reparameterization $K \circ A : T^2 \to \mathscr{T}$ corresponds to the frequency vector $A^{-1}\hat{\omega}$. This implies that the solutions of the system are never isolated. To fix this, we impose a phase condition by requiring that $K(\hat{0})$ is fixed in some way. In the case of a 2D torus and the planar CR3BP, we need two constraint equations. Intuitively, since the 2D torus rotates in two angles, the phase in each angle must be fixed. Recall $K(\theta) = (x, y, \rho_x, \rho_y)^T \in \mathbb{R}^4$. We require $K(\theta)_2 = y = 0$ and $K(\theta)_3 = \rho_x = 0$. If we imagine an orbit on the torus as rotating about a smaller circle and a larger circle, we can imagine the Poincaré map slices the torus along the same plane as the smaller circle. Then the first constraint fixes the rotation about the bigger circle by constraining it to be in the section. The second condition must fix the rotation in the smaller circle. Recall the Poincaré section is a map of (x, ρ_x). By setting $\rho_x = 0$, the point must be on the x-axis. This fixes the phase of K. The constraint equations are

$$K(0,0)_2 = 0$$
$$K(0,0)_3 = 0$$

where the subscripts $K(0,0)_i$ indicate the ith component. Thus, our system of equations to solve becomes,

$$K(0,0)_2 = 0$$
$$K(0,0)_3 = 0$$
$$\omega_1 \frac{\partial}{\partial \theta_1} K(\theta_1, \theta_2) + \omega_2 \frac{\partial}{\partial \theta_2} K(\theta_1, \theta_2) - F(K(\theta)) = 0$$

The system is unbalanced because we have three equations but only one unknown. To balance the system, we introduce a scalar unfolding parameter, α multiplied by the gradient of the Hamiltonian, H. The new system becomes

$$K(0,0)_2 = 0$$
$$K(0,0)_3 = 0$$
$$\omega_1 \frac{\partial}{\partial \theta_1} K(\theta_1, \theta_2) + \omega_2 \frac{\partial}{\partial \theta_2} K(\theta_1, \theta_2) - F(K(\theta)) - \alpha \nabla H(K(\theta_1, \theta_2)) = 0$$

This system is still not fully balanced. Ideally, we would like to add another scalar unfolding parameter, but this is left as something to investigate in future work. Instead, we choose to solve for one of the rotation numbers, ω_2. Then we can define the non-linear mapping Ψ by

$$\Psi(\alpha, \omega_2, K) = \begin{pmatrix} K(0,0)_2 \\ K(0,0)_3 \\ \omega_1 \frac{\partial}{\partial \theta_1} K(\theta_1, \theta_2) + \omega_2 \frac{\partial}{\partial \theta_2} K(\theta_1, \theta_2) - F(K(\theta)) - \alpha \nabla H(K(\theta_1, \theta_2)) \end{pmatrix} \tag{16}$$

Let $\mathbf{0}$ be the 0 vector. Assume Ψ is the operator defined in Eq. (16). Suppose $K_*, \alpha_*, \omega_{2*}$ have

$$\Psi(\alpha_*, \omega_{2*}, K_*) = \begin{pmatrix} 0 \\ 0 \\ \mathbf{0} \end{pmatrix}$$

Then $\alpha_* = 0$, and K_*, ω_{2*} solve Eq. (2).

We proceed to fine a zero of Eq. (16) with a least-squares solution to the Newton step. Let $D\Psi(\alpha, \omega_2, K)$ be the Frechet derivative of Ψ at (α, ω_2, K). Then the Newton step is

$$\begin{pmatrix} \alpha_{n+1} \\ \omega_{2_{n+1}} \\ K_{n+1} \end{pmatrix} = \begin{pmatrix} \alpha_n \\ \omega_{2_n} \\ K_n \end{pmatrix} + \begin{pmatrix} \delta_n \\ \delta_n' \\ \Delta_n \end{pmatrix} \tag{17}$$

where $(\delta_n, \delta_n', \Delta_n)^T$ is a least-squares solution to

$$D\Psi(\alpha_n, \omega_{2_n}, K_n) \begin{pmatrix} \delta_n \\ \delta_n' \\ \Delta_n \end{pmatrix} = -\Psi(\alpha_n, \omega_{2_n}, K_n) \tag{18}$$

Numerically, we let $\mathcal{A}$ be the Moore-Penrose inverse of $D\Psi(\alpha_n, \omega_{2_n}, K_n)$. Then

$$\begin{pmatrix} \delta_n \\ \delta_n' \\ \Delta_n \end{pmatrix} = -\mathcal{A} * \Psi(\alpha_n, \omega_{2_n}, K_n) \tag{19}$$

The spatial case is very similar with the only differences being that the cdomain is now $\mathbb{R}^6$ and the phase conditions are set differently.

Let $\tilde{K}$ be the parameterization of the torus after DFT. Then compute $p = \tilde{K}(0,0)$. The simplest phase condition is $K(0,0)_2 = p_2$ and $K(0,0)_4 = p_4$, where the subscripts indicate the component. We define the nonlinear mapping Ψ by

$$\Psi(\alpha, \omega_2, K) = \begin{pmatrix} K(0,0)_2 - p_2 \\ K(0,0)_4 - p_4 \\ \omega_1 \frac{\partial}{\partial \theta_1} K(\theta_1, \theta_2) + \omega_2 \frac{\partial}{\partial \theta_2} K(\theta_1, \theta_2) - F(K(\theta_1, \theta_2)) - \alpha \nabla H(K(\theta_1, \theta_2)) \end{pmatrix} \tag{20}$$

Like before, the solution of $\Psi(\alpha, \omega_2, K) = \mathbf{0}$ is not isolated. We proceed using a least squares solution as in Eq. (17) - (19).

Numerical Algorithm for Computing QPO Using the Parameterization Method Below we describe the steps for computing a QPO in the planar CR3BP using weighted Birkhoff averaging and the parameterization method.

Step 0: Choose an initial point, p_0, on an invariant circle in the Poincaré map and a point inside the circle q_0. Use the methods mentioned in section *Computing the Rotation Vector* to ensure the point lies on an invariant circle. Then, compute the orbit segment $\text{orbit}_{M,F}(p_0) = \{p_j\}_{j=0}^{M}$ and convert the point data to angle data using Eq. (14) and (15). When computing the orbit, save the return times $\{T_j\}_{j=1}^{M}$.

Step 1: Compute the rotation number, ω, of the invariant circle using Eq. (11). It is important to choose M such that the rotation number converges as close as possible to machine precision. To ensure this, choose a large starting M then increase M by ten or twenty percent and repeat the calculation until convergence is seen in the last digits. Use the same procedure to compute the average flying time using Eq. (13) and ensure convergence in the last digits. See Table 1 for an example of the convergence. Note that the table does not show all the iterations of increasing M.

Step 2: Decide the number of Fourier modes, N, and the length of the orbit, $\tilde{M}$, for $\{x_j\}_{j=0}^{\tilde{M}}$. We want the coefficients to show decay towards zero that is, if $d : \mathbb{N} \to \mathbb{R}$ is defined as

$$d(\alpha) = \{\max(\log(|k_{n,m}|) \, : \, n + m = \alpha\} \quad \alpha = 0, 1, \cdots, 2N$$

we choose N and $\tilde{M}$ so that the d decays to machine precision or saturates. See Figure 2. Note that a larger $\tilde{M}$ will cost in computational time only once to compute all the coefficients, but a larger N will cost more memory in future steps.

Step 3: Choose an initial point on the torus. This can be done by converting the $p_0 = (x_0, \rho_{x_0})$ used in Step 0 into a point in the full phase space, $\tilde{p_0} = (x_0, 0, \rho_{x_0}, \rho_{y_0})$. Iterate the time-1 flow map $\tilde{M}$ times to get a long orbit on the torus, $\{x_j\}_{j=0}^{\tilde{M}}$.

Step 4: Compute the approximate coefficients using weighted Birkhoff averaging with $\{x_j\}_{j=0}^{\tilde{M}}$, Eq. (12), for each $k_{n,m}$, $n = -N, ..., N$ and $m = -N, ..., N$. While the $\tilde{M}$ could be different for each $k_{n,m}$, it usually does not make a difference in computational time since the bottleneck is governed by the computation of the orbit which only has to be computed once for all of the $k_{n,m}$.

Step 5: Perform the Newton scheme outlined above on the mapping Eq. (16) until the defect

$$\epsilon = \sup_{\theta \in [0,1]^2} |F(K(\theta)) - DK(\theta)\hat{\omega}| \tag{21}$$

saturates or decreases below some desired tolerance.

The previous steps describe the method for the planar case. In the spatial case, the algorithm is as follows:

Step 0: Choose whether the orbit will be an L_1 or L_2 Lissajous orbit and choose values for I_2 and I_3. Set $I_1 = 0$. Generate the torus using Local Orbital Element Toolkit with $2N + 1$ points in each angle. The value of N becomes the number of Fourier modes which should be chosen so the coefficients decay past some tolerance level or saturate.

Step 1: Compute the rotation numbers ω_1, ω_2 as described at the end of *Computing the Rotation Vector*.

Step 2: Same as step 5 for the planar case but using Eq. (20).

Newton Method Set-up for Stable/Unstable Manifolds

The method is the same for the stable and unstable manifolds, so we will only refer to the stable, but the same applies to the unstable. The goal is to solve for the Fourier-Taylor series of Q as in Eq. (5) that solves Eq. (4). Once we have computed the torus, K which becomes the a_0 coefficient in the expansion of Q we compute the invariant vector bundle, which is just the $a_1(\theta)$ coefficient. Then to compute a_n for $n \geq 2$ we use a 'power-matching' method to compute each coefficient order-by-order. Kumar, Anderson, and de la Llave also computed coefficients of the Fourier-Taylor series expansion of a manifold order-by-order; however they employ automatic differentiation and jet transport in computing each term.[17] Here, we compute the coefficients using a Newton scheme for each order. By noticing that the nth coefficient of the expansion of $F(Q)$ can be written as $DF(a_0)a_n + R_n(a_0, ..., a_{n-1})$, we can easily differentiate $F(Q)$ with respect to a_n and perform Newton.

We write Q as a Fourier-Taylor series

$$Q(\theta_1, \theta_2, \sigma) = \sum_{n=0}^{\infty} a_n(\theta_1, \theta_2)\sigma^n \tag{22}$$

where each $a_n : \mathbb{T}^2 \to \mathbb{R}^6$ is a Fourier series and

$$a_0(\theta_1, \theta_2) = K(\theta_1, \theta_2)$$
$$a_1(\theta_1, \theta_2) = B(\theta_1, \theta_2)$$

With $K(\theta_1, \theta_2)$ satisfying (2) and $B(\theta_1, \theta_2)$ satisfying (6) with the associated Floquet multiplier λ.

We solve for B by applying a Newton scheme on the linear operator defined in Eq. (7). The bundle, B, is not isolated since any scale multiple of B is also a solution. Thus, we fix the length of the bundle

$$||B||^2_{L^2} - c = 0$$

where c is some constant we choose. If we solve for B and λ, the equation becomes balanced, and we can apply a Newton scheme to the system

$$-\omega_1 \frac{\partial}{\partial \theta_1} B - \omega_2 \frac{\partial}{\partial \theta_2} B + DF(K(\theta))B - \lambda B = 0 \tag{23}$$
$$||B||^2_{L^2} - c = 0 \tag{24}$$

The initial guess for B and λ is computed using MATLAB's built-in eig function on Eq. (7). See Figure 5 for an example of the torus with the invariant bundle showing the direction of the manifold.

For the rest of the coefficients of Q, $n \geq 2$, we employ a 'power matching' scheme. Suppose that $F(Q)$ can be written as a Fourier-Taylor series

$$F(Q(\theta_1, \theta_2, \sigma)) = \sum_{n=0}^{\infty} b_n(\theta_1, \theta_2)\sigma^n \tag{25}$$

where each $b_n : \mathbb{T}^2 \to \mathbb{R}^6$ is a Fourier series. This composition of a trigonometric polynomial with the (non-polynomial) vector field, F, is computed used FFT.

Consider the expansion of each term on the right-hand side of Eq. (4)

$$\begin{aligned}
\omega_1 \frac{\partial}{\partial \theta_1} Q(\theta_1, \theta_2, \sigma) &= \sum_{n=0}^{\infty} \omega_1 \frac{\partial}{\partial \theta_1} a_n(\theta_1, \theta_2)\sigma^n \\
\omega_2 \frac{\partial}{\partial \theta_2} Q(\theta_1, \theta_2, \sigma) &= \sum_{n=0}^{\infty} \omega_2 \frac{\partial}{\partial \theta_2} a_n(\theta_1, \theta_2)\sigma^n \\
\lambda\sigma \frac{\partial}{\partial \sigma} Q(\theta_1, \theta_2, \sigma) &= \sum_{n=0}^{\infty} n\lambda a_n(\theta_1, \theta_2)\sigma^n
\end{aligned}$$

Substituting this back into the Eq. (4) results in

$$\sum_{n=0}^{\infty} \left(\omega_1 \frac{\partial}{\partial \theta_1} a_n(\theta_1, \theta_2) + \omega_2 \frac{\partial}{\partial \theta_2} a_n(\theta_1, \theta_2) + n\lambda a_n(\theta_1, \theta_2) \right) \sigma^n = \sum_{n=0}^{\infty} b_n(\theta_1, \theta_2)\sigma^n$$

Matching the coefficients of σ^n on both sides, we have

$$\omega_1 \frac{\partial}{\partial \theta_1} a_n(\theta_1, \theta_2) + \omega_2 \frac{\partial}{\partial \theta_2} a_n(\theta_1, \theta_2) + n\lambda a_n(\theta_1, \theta_2) = b_n(\theta_1, \theta_2) \quad n = 2, 3, ...$$

Define the linear operator $L : C(\mathbb{T}^2, \mathbb{R}^6) \to C(\mathbb{T}^2, \mathbb{R}^6)$ that acts on a_n by

$$L[a_n] := \omega_1 \frac{\partial}{\partial \theta_1} a_n + \omega_2 \frac{\partial}{\partial \theta_2} a_n + n\lambda a_n$$

To solve for a_n, we solve $La_n = b_n$. For $n \geq 2$, L is a nonzero diagonal matrix, thus invertible. We write $a_n = L^{-1}b_n$. The goal is to solve for the a_n's using a Newton-like scheme on

$$\Xi(a_n) = a_n - L^{-1}b_n \tag{26}$$

How do we differentiate this with respect to a_n? Consider the Taylor expansion of $F(Q)$ about $\sigma = 0$.

$$F(Q(\theta_1, \theta_2, \sigma)) = \sum_{n=0}^{\infty} \frac{1}{n!} \frac{\partial^n}{\partial \sigma^n} \left[F(Q(\theta_1, \theta_2, \sigma)) \right]_{\sigma=0} \sigma^n$$

Plugging in Q as its series (Eq. (22)) and simplifying the notation results in

$$\begin{aligned}
&\sum_{n=0}^{\infty} \frac{1}{n!} \frac{\partial^n}{\partial \sigma^n} \left[F\left(\sum_{m=0}^{\infty} a_m \right) \right]_{\sigma=0} \sigma^n \\
&= F(a_0) + DF(a_0)a_1\sigma + \frac{1}{2}(D^2F(a_0)a_1 + 2DF(a_0)a_2)\sigma^2 + \cdots \\
&= \sum_{n=0}^{\infty} \left(DF(a_0)a_n + R_n(a_0, a_1, \cdots, a_{n-1}) \right) \sigma^n \\
&= \sum_{n=0}^{\infty} b_n\sigma^n
\end{aligned}$$

where R_n is a function of only $a_0, a_1, ..., a_{n-1}$. By matching coefficients,

$$b_n = DF(a_0)a_n + R_n(a_0, a_1, \cdots, a_{n-1})$$

Thus, the only dependence on a_n is in the $DF(a_0)a_n$ term. Then we have,

$$D\Xi(a_n) = I - L^{-1}DF(a_0)$$

Since we expect the norm of a_n to decay as n increases, we use $a_n = 0$ as the initial guess for a_n for $n \geq 2$.

Numerical Algorithm for Computing Unstable (Stable) Manifolds around a QPO Using the Parameterization Method Below we outline the steps for computing the stable or unstable manifolds attached to a QPO.

Step 0: Compute the QPO for the spatial problem as detailed in the *Numerical Algorithm for Computing QPO Using the Parameterization Method.* This is $K(\theta) = a_0(\theta)$ the first Taylor coefficient.

Step 1: Use MATLAB's (or some other program's) eigenvalue function on Eq. (7).

Step 2: Choose the eigenvalue/eigenfunction pair whose eigenvalue has the smallest imaginary part and the real part is positive. For the stable case, use the same criteria but with the real part negative. The eigenfunction becomes $B(\theta) = a_1(\theta)$ the unstable vector bundle with Floquet multiplier λ, the eigenvalue.

Step 3: Correct the unstable bundle/eigenvalue pair. Perform a Newton method on the system of equations Eq. (23)-(24) until the defect

$$\epsilon = \sup_{\theta \in [0,1]^2} \left| -\omega_1 \frac{\partial}{\partial \omega_1} B(\theta) - \omega_2 \frac{\partial}{\partial \omega_2} B(\theta) + DF(K(\theta))B(\theta) - \lambda B(\theta) \right|$$

saturates or decreases below some desired tolerance.

Step 4: Choose how many Taylor modes, M_T, of the manifold to compute. Set the first two coefficients to K and B respectively. For each $n = 2, ..., M_T$, set the initial guess to $a_n(\theta) = \mathbf{0}$. To compute b_n, the coefficients of $F(Q(\theta_1, \theta_2, \sigma))$, using FFT, then perform a Newton method on Eq. (26) until the defect

$$\epsilon = \sup_{\theta \in [0,1]^2} \left| a_n(\theta) - L^{-1} b_n(\theta) \right|$$

NUMERICAL RESULTS

Planar CR3BP: Quasi-Periodic Lunar Distant Retrograde Orbit

The results for the planar CR3BP are shown in Figure 1, Figure 2, and Table 1. The torus was computed with $N = 20$ Fourier modes which was chosen based on the decay of the coefficients. After 20, it begins to saturate. Each coefficient was computed using the algorithm detailed in the previous sections with $\tilde{M} = 30000$ for all coefficients. After 4 iterations of the Newton scheme, the step size is of the order of 10^{-12} and the Fourier coefficients of the corrected torus decay to 10^{-18}. On an AMD Ryzen AI 9 365 with Radeon 880M, 2000 Mhz, 10 Cores, and 24 GB of RAM, the correction of the torus took about 5.4 minutes.

M	ω_M	T_M
2000	0.0892421925212603	0.5454416402608680
5000	0.0892421844205661	0.5454416402608730
10000	0.0892421844586325	0.5454416402605470
15000	0.0892421844586122	0.5454416402603640
20000	0.0892421844585820	0.5454416402601790
25000	0.0892421844585492	0.5454416402599700
30000	0.0892421844585217	0.5454416402598080

Table 1: Convergence of the rotation number of the Poincaré map, ω_M, and the average return time T_M using Eq (11) and Eq (13). The computation was for the same torus shown in Figure 1.

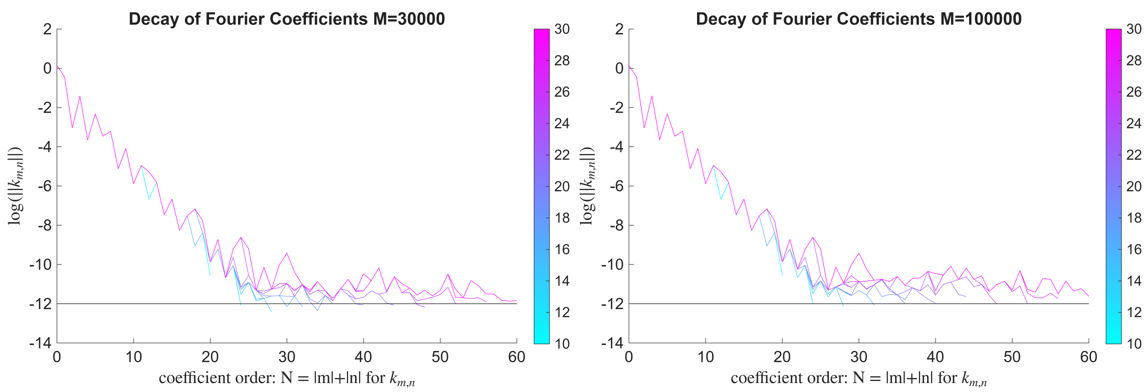

Figure 2: Decay of the log of the magnitude of the Fourier coefficients for varying number of Fourier modes from 10 to 30. Coefficients were computed using Eq (12) with $M = 30000$ and $M = 100000$. The black line is at -12. Notice that after around 20 modes, it saturates and no longer decays. The difference in the two graphs is minimal indicating that taking a longer orbit, which is computationally expensive, is not a significant benefit since it will be corrected.

Table 2: Table of computational results for spatial tori.

$I_1 = 0 \quad I_3 = 0.05 \quad \text{Tol} = 10^{-14}$							
I_2	N	Time	Iterations	Init Defect	Final Defect	Init Fourier Decay	Final Fourier Decay
0.015	12	106 sec	6	10^{-3}	10^{-15}	10^{-6}	10^{-17}
0.04	12	106 sec	6	10^{-3}	10^{-16}	10^{-6}	10^{-17}
0.065	12	93 sec	6	10^{-3}	10^{-16}	10^{-6}	10^{-15}
0.09	12	93 sec	6	10^{-2}	10^{-16}	10^{-6}	10^{-13}
0.115	12	93 sec	6	10^{-2}	10^{-16}	10^{-6}	10^{-12}

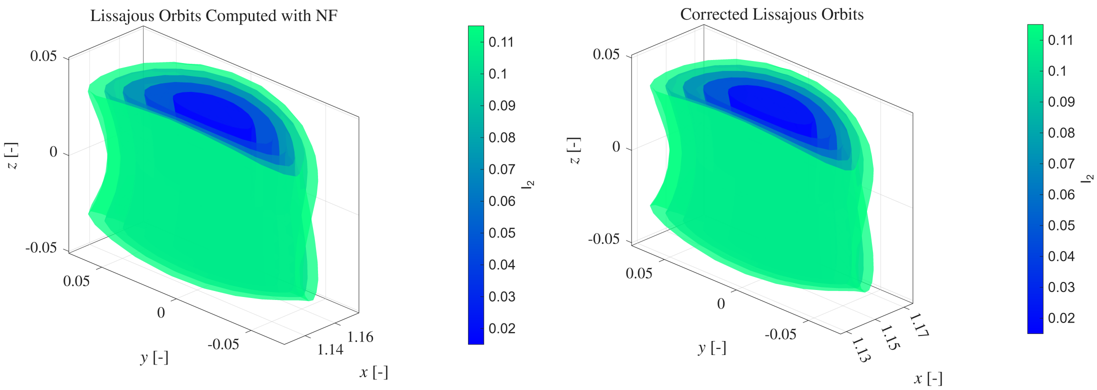

Figure 3: The left shows five QPOs computed using normal form decomposition and the right shows the result after the correction. Observe that the normal form initial guesses look nearly identical to their corrected versions, indicating not only that the normal form provides a good initial guess, but also that the parameterization method preserves the relative orbit geometry well.

Spatial CR3BP: L_2 Lissajous Orbit

Table 2 shows the computational results for computing five different tori with $I_1 = 0$, $I_3 = 0.05$ and varying I_2. The same number of Fourier modes were used for each and all the computations were run on the same computer as before.

For the computation of the unstable bundle, the system is very close to linear, so the initial defect is of the order 10^{-10} and after only 3 iterations, the defect is at machine precision, 10^{-16}. The computation is similar for the stable bundle as well see Figure 4. Figure 5 shows the unstable manifold as it departs from the quasi-periodic orbit. The manifold was computed with 12 Fourier modes in each angle and 20 Taylor modes. The first gray torus represents the manifold evaluated at $\sigma = 1$ and the other snapshots are computed by integrating 625 points forward in time.

CONCLUDING REMARKS

In this paper, we presented a numerical method for computing quasi-periodic invariant tori in the CR3BP using the parameterization method. This method uses a Newton like scheme that solves for the Fourier coefficients of the parameterization of the torus. To compute the rotation vector and generate an initial approximation, we use the Weighted Birkhoff Average in the planar case and the normal form in the spatial case. We also presented a method for computing high-order Fourier-Taylor expansions of the stable and unstable manifolds associated with the invariant tori. Once the torus is computed, we compute the invariant bundle and Floquet multiplier. These, together with the torus become the first order coefficients for the manifold. Then we solve for the other Taylor coefficients order-by-order using DFT combined with a 'power-matching' method. This avoids using a large matrix method which solves for all the coefficients at once and is computationally expensive. By computing the coefficients in this way we can quickly compute higher orders without a significant cost of memory.

One area of improvement to explore is in decreasing the computation time for the invariant torus. Although more Fourier modes generally result in a better approximation, it increases the size of the matrix used in the Newton scheme which in turn increases the memory usage. This could become

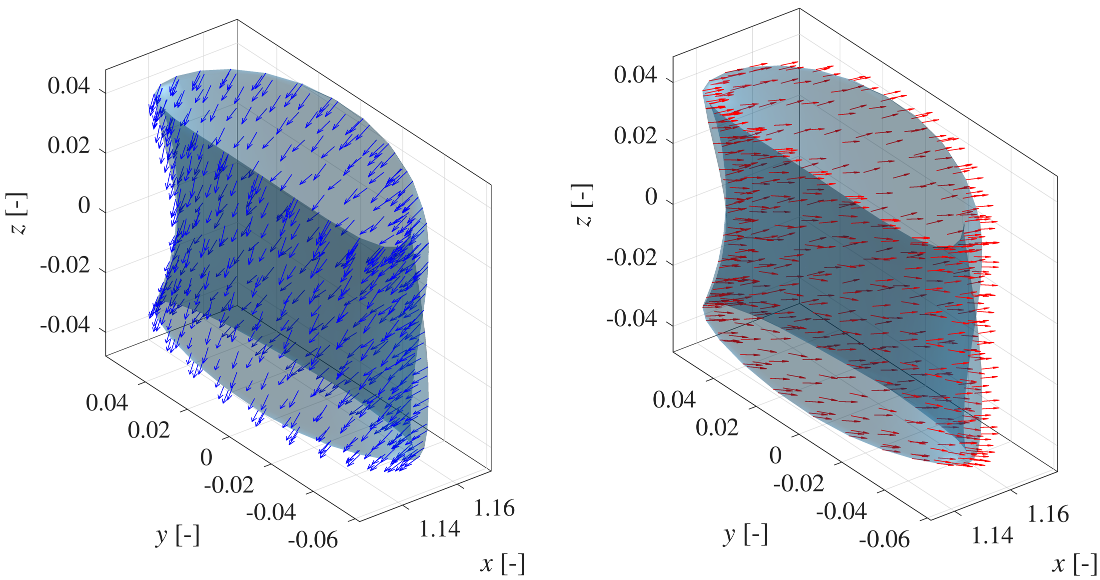

Figure 4: The quasi-periodic orbit with attached stable (blue) and unstable (red) bundles.

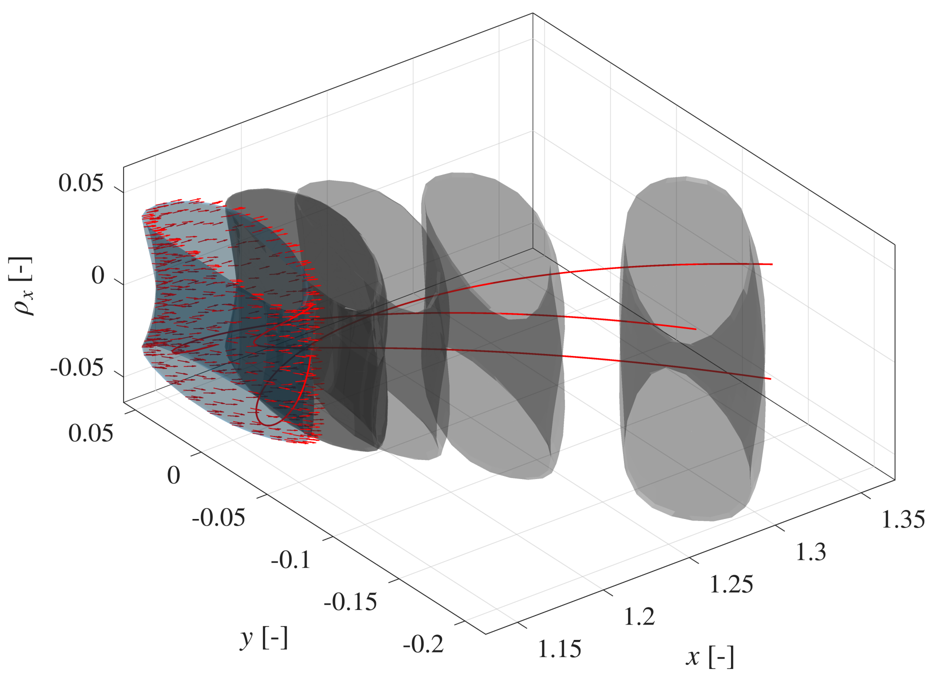

Figure 5: Snapshots of the unstable manifolds (gray) departing the quasi-periodic orbit (blue). the unstable bundle is represented by the red arrows.

a problem especially if one were to extend this work to higher dimensional tori. A future project could be to examine how to diagonalize the derivative in the Newton scheme for faster computation and allow for more Fourier modes.

Another area of interest is the search for homoclinic connecting orbits. Kepley and Mireles-James developed a method for finding connecting orbits by growing charts for the stable and unstable manifolds of an invariant curve.[38] Since our method of computing manifolds computes the whole manifold in phase space instead of just in a section, it is ideal for combining with Kepley and Mireles-James' method to grow manifolds in higher dimensions and find connecting orbits.

REFERENCES

[1] R. Farquhar, D. Muhonen, and L. Church, "Trajectories and orbital maneuvers for the ISEE-3/ICE comet mission," *Astrodynamics conference*, 1984, p. 1976.

[2] T. Gardner, B. Cheetham, J. Parker, A. Forsman, E. Kayser, M. Thompson, C. Ott, L. DeMoudt, M. Caudill, M. Bolliger, A. Kam, K. Thompson, R. Rogers, H. Umansky, B. Bryant, and T. Svitek, "CAPSTONE: A Summary of a Highly Successful Mission in the Cislunar Environment," *37th Annual Small Satellite Conference*, Logan, UT, 2023.

[3] A. L. Batcha, J. Williams, T. F. Dawn, J. P. Gutkowski, M. V. Widner, S. L. Smallwood, B. J. Killeen, E. C. Williams, and R. E. Harpold, "Artemis I trajectory design and optimization," *2020 AAS/AIAA Astrodynamics Specialist Conference*, No. AAS 20-649, 2020.

[4] J. P. Sánchez, D. Morante, P. Hermosin, D. Ranuschio, A. Estalella, D. Viera, S. Centuori, G. Jones, C. Snodgrass, A. C. Levasseur-Regourd, *et al.*, "Esa f-class comet interceptor: trajectory design to intercept a yet-to-be-discovered comet," *Acta Astronautica*, Vol. 188, 2021, pp. 265–277.

[5] S. Fuller, E. Lehnhardt, C. Zaid, and K. Halloran, "Gateway program status and overview," *Journal of Space Safety Engineering*, Vol. 9, No. 4, 2022, pp. 625–628.

[6] C. E. Roberts, "Long term missions at the sun-earth libration point l1: Ace, soho, and wind," *AAS/AIAA Astrodynamics Specialist Conference*, No. GSFC. CP. 4786.2011, 2011.

[7] C. Roberts, S. Case, J. Reagoso, and C. Webster, "Early mission maneuver operations for the deep space climate observatory Sun-Earth L1 libration point mission," *AIAA/AAS Astrodynamics Specialist Conference*, No. GSFC-E-DAA-TN25055, 2015.

[8] R. L. Restrepo, R. P. Russell, M. W. Lo, and T. P. McElarth, "Europa lander trajectory design using Lissajous staging orbits," *AAS/AIAA Astrodynamics Specialist Conference, Snowbird, Utah*, 2018.

[9] B. T. Barden and K. C. Howell, "Fundamental motions near collinear libration points and their transitions," *The Journal of the Astronautical Sciences*, Vol. 46, No. 4, 1998, pp. 361–378.

[10] N. Baresi, *Spacecraft formation flight on quasi-periodic invariant tori*. PhD thesis, University of Colorado at Boulder, 2017.

[11] G. Gómez, J. Llibre, R. Martínez, and C. Simó, *Dynamics and mission design near libration points. Vol. I.*, Vol. 2 of *World Scientific Monograph Series in Mathematics*. World Scientific Publishing Co., Inc., River Edge, NJ, 2001. Fundamentals: the case of collinear libration points, With a foreword by Walter Flury, 10.1142/9789812810632_bmatter.

[12] G. Gómez, C. Simó, J. Llibre, and R. Martínez, *Dynamics and mission design near libration points. Vol. II*, Vol. 3 of *World Scientific Monograph Series in Mathematics*. World Scientific Publishing Co., Inc., River Edge, NJ, 2001. Fundamentals: the case of triangular libration points.

[13] G. Gómez, A. Jorba, C. Simó, and J. Masdemont, *Dynamics and mission design near libration points. Vol. III*, Vol. 4 of *World Scientific Monograph Series in Mathematics*. World Scientific Publishing Co., Inc., River Edge, NJ, 2001. Advanced methods for collinear points.

[14] G. Gómez, A. Jorba, C. Simó, and J. Masdemont, *Dynamics and mission design near libration points. Vol. IV*, Vol. 5 of *World Scientific Monograph Series in Mathematics*. World Scientific Publishing Co., Inc., River Edge, NJ, 2001. Advanced methods for triangular points.

[15] A. Jorba and E. Olmedo, "On the computation of reducible invariant tori on a parallel computer," *SIAM Journal on Applied Dynamical Systems*, Vol. 8, No. 4, 2009, pp. 1382–1404.

[16] G. Gómez and J. M. Mondelo, "The dynamics around the collinear equilibrium points of the RTBP," *Physica D: Nonlinear Phenomena*, Vol. 157, No. 4, 2001, pp. 283–321.

[17] B. Kumar, R. L. Anderson, and R. d. l. Llave, "Rapid and accurate methods for computing whiskered tori and their manifolds in periodically perturbed planar circular restricted 3-body problems," *Celestial Mechanics and Dynamical Astronomy*, Vol. 134, No. 1, 2022, p. 3.

[18] F. Schilder, H. M. Osinga, and W. Vogt, “Continuation of quasi-periodic invariant tori,” *SIAM Journal on Applied Dynamical Systems*, Vol. 4, No. 3, 2005, pp. 459–488.

[19] N. Baresi, Z. P. Olikara, and D. J. Scheeres, “Fully numerical methods for continuing families of quasi-periodic invariant tori in astrodynamics,” *The Journal of the astronautical sciences*, Vol. 65, No. 2, 2018, pp. 157–182.

[20] A. Haro and J.-M. Mondelo, “Flow map parameterization methods for invariant tori in Hamiltonian systems,” *Communications in Nonlinear Science and Numerical Simulation*, Vol. 101, 2021, p. 105859.

[21] S. Das, Y. Saiki, E. Sander, and J. A. Yorke, “Quantitative quasiperiodicity,” *Nonlinearity*, Vol. 30, No. 11, 2017, pp. 4111–4140.

[22] E. Sander and J. D. Meiss, “Birkhoff averages and rotational invariant circles for area-preserving maps,” *Physica D: Nonlinear Phenomena*, Vol. 411, 2020, p. 132569.

[23] D. Blessing and J. D. Mireles James, “Weighted Birkhoff averages and the parameterization method,” *SIAM Journal on Applied Dynamical Systems*, Vol. 23, No. 3, 2024, pp. 1766–1804.

[24] O. Boodram, D. Henry, and D. Scheeres, “RAPID COMPUTATION AND IDENTIFICATION OF ROTATIONAL INVARIANT CURVES ON THE KEPLERIAN MAP,”

[25] M. Ruth, J. Kulik, and J. Burby, “Robust computation of higher-dimensional invariant tori from individual trajectories,” *Chaos: An Interdisciplinary Journal of Nonlinear Science*, Vol. 36, No. 3, 2026.

[26] A. D. Perry and S. Wiggins, “KAM tori are very sticky: rigorous lower bounds on the time to move away from an invariant Lagrangian torus with linear flow,” *Physica D: Nonlinear Phenomena*, Vol. 71, No. 1-2, 1994, pp. 102–121.

[27] A. Jorba and J. Masdemont, “Dynamics in the center manifold of the collinear points of the restricted three body problem,” *Physica D: Nonlinear Phenomena*, Vol. 132, No. 1-2, 1999, pp. 189–213.

[28] À. Jorba, “A methodology for the numerical computation of normal forms, centre manifolds and first integrals of Hamiltonian systems,” *Experimental Mathematics*, Vol. 8, No. 2, 1999, pp. 155–195.

[29] À. Jorba and J. Villanueva, “Numerical Computation of Normal Forms around some Periodic Orbits of the Restricted Three-Body Problem,” *Physica D: Nonlinear Phenomena*, Vol. 114, No. 3-4, 1998, pp. 197–229.

[30] L. Peterson and D. Scheeres, “Local Orbital Element Toolkit in Cislunar Space,” *AAS/AIAA Astrodynamics Specialist Conference, Broomfield, Colorado, Aug*, Vol. 12, 2024.

[31] J. Gimeno and L. T. Peterson, “Effective Stability of Near-Rectilinear Halo Orbits in the Earth-Moon System,” *arXiv e-prints*, Apr. 2026, p. arXiv:2604.02466, 10.48550/arXiv.2604.02466.

[32] V. Szebehely, *Theory of orbit: The restricted problem of three Bodies*. Elsevier, 2012.

[33] X. Cabré, E. Fontich, and R. D. l. Llave, “The parameterization method for invariant manifolds I: manifolds associated to non-resonant subspaces,” *Indiana University mathematics journal*, 2003, pp. 283–328.

[34] X. Cabré, E. Fontich, and R. D. l. Llave, “The parameterization method for invariant manifolds II: regularity with respect to parameters,” *Indiana University mathematics journal*, 2003, pp. 329–360.

[35] X. Cabré, E. Fontich, and R. De La Llave, “The parameterization method for invariant manifolds III: overview and applications,” *Journal of Differential Equations*, Vol. 218, No. 2, 2005, pp. 444–515.

[36] A. Haro, M. Canadell, J.-L. Figueras, A. Luque, and J.-M. Mondelo, *The parameterization method for invariant manifolds*, Vol. 195. Springer, 2016.

[37] J. Laskar, C. Froeschlé, and A. Celletti, “The measure of chaos by the numerical analysis of the fundamental frequencies. Application to the standard mapping,” *Physica D: Nonlinear Phenomena*, Vol. 56, No. 2-3, 1992, pp. 253–269.

[38] S. Kepley and J. D. M. James, “Homoclinic dynamics in a restricted four body problem,” 2019.